FE homogenized limit analysis code for masonry buildings

By

Gabriele Milani[*] and Paulo B. Lourenço[+]

[*] Corresponding author. Assistant Professor. Dipartimento di Ingegneria Strutturale (DIS), Politecnico di Milano, Piazza Leonardo da Vinci 32, 20133 Milano. E-mail: milani@stru.polimi.it. Phone: +39 3495516064

[+] Full Professor. Department of Civil Engineering (DEC), University of Minho, Azurém, P-4800-058 Guimarães, Portugal. E-mail: pbl@civil.uminho.pt

Number of words: 3640

Number of figures: 9

Number of tables: 2

1

Abstract

In this paper, a FE homogenized limit analysis code for the collapse analysis of 3D masonry buildings subjected to horizontal actions is presented. In the code, masonry is modelled through a fictitious macroscopic homogeneous material. Masonry macroscopic mechanical properties are obtained by means of a recently presented equilibrated limit analysis approach performed on a suitable unit cell, which generates the entire structure by repetition. Masonry homogenised failure surfaces are then implemented in the 3D code here outlined. With respect to previously presented models, the algorithm allows to analyze real scale buildings for coupled in-plane and out-of-plane actions. The possible presence of steel, RC and ring beams is also considered introducing in the numerical model two-node beam elements. A relevant 3D structural example consisting of a masonry school subjected to horizontal actions is treated. Full sensitivity analyses and a comparison with results obtained with a commercial elasto-plastic software are also presented to validate the model proposed.

1   Introduction

The evaluation of the ultimate load bearing capacity of masonry buildings subjected to horizontal loads is a fundamental task in their design or safety assessment. Simplified limit analysis methods are usually adopted by practitioners for safety analyses and design of strengthening [1], but codes of practice, as for instance the recent Italian O.P.C.M. 3431 [2,3], require a static non linear analysis for existing masonry buildings, in which a limited ductile behaviour of the elements is taken into account, featuring failure mechanisms such as rocking, shear and diagonal cracking of the walls.

In this framework, many researchers tried to propose a number of different numerical approaches (see [4] for a comprehensive review), based on micro-modelling, macro-modelling or homogenisation, with the aim of obtaining reliable tools to predict masonry behaviour at failure.

However, heterogeneous approaches [5], which are based on a distinct representation of bricks and joints, seem limited to the study of panels of small dimensions, due to the large number of variables involved in a non linear finite element analysis. On the other hand, strategies based on macro-modelling [6] have the drawback of requiring a preliminary mechanical characterization of the model, which usually is obtained from experimental data fitting. The present paper focuses exclusively on the collapse analysis of masonry structures making use of homogenisation techniques. Such an approach is based on the substitution of the heterogeneous material by a fictitious homogeneous one, with mechanical properties calibrated on a representative element of volume that generates the entire structure by repetition. For this reason, it seems to be the only approach suitable to be employed in a large scale finite element analysis. Furthermore, the application of homogenisation theory to the rigid-plastic case [7] is particularly indicated for a simple but reliable structural analysis, requiring only a reduced number of material parameters and providing significant information at failure, such as limit multipliers, collapse mechanisms and, at least on critical sections, the stress distribution [8].

In this paper, the micro-mechanical model presented by the authors in [8,9] and [10] for the limit analysis of respectively in- and out-of-plane loaded masonry walls is generalized and utilized for the analysis of a 3D real masonry building in presence of coupled membrane and flexural effects. In the model, the elementary cell is subdivided along its thickness in several layers. For each layer, fully equilibrated stress fields are assumed, adopting polynomial expressions for the stress tensor components in a finite number of sub-domains. The continuity of the stress vector on the interfaces between adjacent sub-domains and suitable anti-periodicity conditions on the boundary surface are further imposed. In this way, linearised homogenised surfaces in six dimensions for masonry in- and out-of-plane loaded are obtained. Such surfaces are then implemented in a FE limit analysis code for the analysis at collapse of 3D structures.

The code has an easy-to-use graphical interface, which allows to model directly masonry piers and spandrels by means of triangular plate and shell elements. Steel and RC beams are suitably considered through the introduction of two-node 1D rigid-plastic beam elements.

A relevant 3D structural example consisting of a masonry school subjected to horizontal actions is treated. Full sensitivity analyses and a comparison with results obtained with a commercial elasto-plastic software are also presented to validate the model proposed.

2 In- and out-of-plane masonry homogenised failure surfaces

In order to have an estimation of masonry macroscopic failure surfaces, homogenisation concepts are hereafter applied, assuming for the constituent materials (bricks and mortar) a rigid-perfectly plastic behaviour with associated flow rule.

Let S^m, S^b and S^{hom} denote respectively the strength domains of mortar, units and homogenised macroscopic material. It has been shown by Suquet [7] in a general framework that the S^{hom} can be obtained by means of a so-called static approach, in which the variables to handle are the stresses on the unit cell (hereafter called micro-stresses). The authors recently proposed [9, 10] a simplified procedure to obtain homogenised in- and out-of-plane failure surfaces S^{hom} for masonry. In particular, S^{hom} has been derived by means of the following (non-linear) optimization problem:

$$S^{hom} = \left\{ \max(\mathbf{M}, \mathbf{N}) \mid \begin{cases} \mathbf{N} = \dfrac{1}{|Y|} \displaystyle\int\limits_{Y \times h} \boldsymbol{\sigma} dV & (a) \\ \mathbf{M} = \dfrac{1}{|Y|} \displaystyle\int\limits_{Y \times h} y_3 \boldsymbol{\sigma} dV & (b) \\ div\boldsymbol{\sigma} = \mathbf{0} & (c) \\ [\![\boldsymbol{\sigma}]\!] \mathbf{n}^{int} = \mathbf{0} & (d) \\ \boldsymbol{\sigma}\mathbf{n} \quad \text{anti-periodic} \quad \text{on} \quad \partial Y_l & (e) \\ \boldsymbol{\sigma}(\mathbf{y}) \in S^m \quad \forall \mathbf{y} \in Y^m ; \ \boldsymbol{\sigma}(\mathbf{y}) \in S^b \quad \forall \mathbf{y} \in Y^b & (f) \end{cases} \right\} \quad (1)$$

where:
- $\mathbf{N}$ and $\mathbf{M}$ are the macroscopic in-plane (membrane forces) and out-of-plane (bending moments and torsion) tensors;
- $\boldsymbol{\sigma}$ denotes the microscopic stress tensor;
- $\mathbf{n}$ is the outward versor of ∂Y_l surface, see Figure 1-a;
- $[\![\boldsymbol{\sigma}]\!]$ is the jump of micro-stresses across any discontinuity surface of normal $\mathbf{n}^{int}$, Figure 1-c;
- S^m and S^b denote respectively the strength domains of mortar and bricks;
- Y is the cross section of the 3D elementary cell with $y_3 = 0$ (see Figure 1), $|Y|$ is its area, V is the elementary cell volume, h represents the wall thickness and $\mathbf{y} = \begin{pmatrix} y_1 & y_2 & y_3 \end{pmatrix}$ are the assumed material axes;
- Y^m and Y^b represent mortar joints and bricks respectively, see Figure 1.

It is worth noting that anti-periodicity conditions (1-e) require that that stress vectors $\boldsymbol{\sigma}$ ₁ are opposite on opposite sides of ∂Y_l, Figure 1-c, i.e. $\sigma^{(m)}\mathbf{n}_1 = -\sigma^{(n)}\mathbf{n}_2$

4

In a previous work by the authors [8], the unit cell was subdivided into a fixed number of layers along its thickness, as shown in Figure 1-b. For each layer out-of-plane components σ_{i3} ($i = 1, 2, 3$) of the micro-stress tensor $\boldsymbol{\sigma}$ were set to zero, so that only in-plane components σ_{ij} ($i, j = 1, 2$) were considered active. Furthermore, σ_{ij} ($i, j = 1, 2$) were kept constant along the Δ_L thickness of each layer L, i.e. in each layer $\sigma_{ij} = \sigma_{ij}(y_1, y_2)$. For each layer in the wall thickness direction, one-fourth of the representative volume element was sub-divided into nine geometrical elementary entities (sub-domains), so that the entire elementary cell was sub-divided into 36 sub-domains [9] (see Figure 1-b).

For each sub-domain (k) and layer (L), polynomial distributions of degree (m) in the variables (y_1, y_2) were a priori assumed for the stress components. Since stresses were polynomial expressions, the generic ij th component was written as follows:

$$\sigma_{ij}^{(k,L)} = \mathbf{X}(\mathbf{y})\mathbf{S}_{ij}^{(k,L)T} \quad \mathbf{y} \in Y^{(k,L)} \tag{2}$$

where:

- $\mathbf{X}(\mathbf{y}) = \begin{bmatrix} 1 & y_1 & y_2 & y_1^2 & y_1 y_2 & y_2^2 & \ldots \end{bmatrix}$;

- $\mathbf{S}_{ij}^{(k,L)} = \begin{bmatrix} S_{ij}^{(k,L)(1)} & S_{ij}^{(k,L)(2)} & S_{ij}^{(k,L)(3)} & S_{ij}^{(k,L)(4)} & S_{ij}^{(k,L)(5)} & S_{ij}^{(k,L)(6)} & \ldots \end{bmatrix}$ is a vector representing the unknown stress parameters of sub-domain (k) of layer (L);

- $Y^{(k,L)}$ represents the k th sub-domain of layer (L).

The imposition of equilibrium inside each sub-domain, the continuity of the stress vector on interfaces and the anti-periodicity of $\boldsymbol{\sigma}\,\mathbf{n}$ permitted a reduction in the number of independent stress parameters [9].

Assemblage operations on the local variables allowed to write the stress vector $\tilde{\boldsymbol{\sigma}}^{(k,L)}$ of layer L inside each sub-domain as:

$$\tilde{\boldsymbol{\sigma}}^{(k,L)} = \tilde{\mathbf{X}}^{(k,L)}(\mathbf{y})\tilde{\mathbf{S}}^{(L)} \quad k = 1, \ldots, \text{ no. of sub-domains } L = 1, \ldots, \text{ no. of layers} \tag{3}$$

where $\tilde{\mathbf{S}}^{(L)}$ is a $N_{uk} x 1$ ($N_{uk} = $ number of unknowns per layer) vector of linearly independent unknown stress parameters of layer L and $\tilde{\mathbf{X}}^{(k,L)}(\mathbf{y})$ is a $3 x N_{uk}$ matrix depending only on the geometry of the elementary cell and on the position $\mathbf{y}$ of the point in which the micro-stress is evaluated.

3   3D kinematic FE limit analysis: basic assumptions

Masonry homogenized strength domain obtained with the simple model summarized in the previous section are implemented in a novel and optimized 3D kinematic FE limit analysis code for the analysis at collapse of entire buildings.

The upper bound approach here proposed is based both on the formulation presented in Sloan and Kleeman [11] for the in-plane case and on the formulation by Munro and Da Fonseca [12] for out-of-plane actions. The formulation uses three-node triangular elements with linear interpolation of the velocity field inside each element, so that

three velocity unknowns per node i, say w_{xx}^i, w_{yy}^i and w_{zz}^i (respectively two in-plane velocities and one out-of-plane velocity, see Figure 2-a) are introduced for each element E, meaning that the velocity field is linear inside an element, whereas the strain rate field is constant for in-plane actions.

For the sake of simplicity, it is assumed that jump of velocities on interfaces occurs only in the plane containing two contiguous and coplanar elements, with linear interpolation of the jump along the interface. Hence, for each interface between coplanar adjacent elements, four additional unknowns are introduced ($\Delta \mathbf{u}^I = \begin{bmatrix} \Delta v_1 & \Delta u_1 & \Delta v_2 & \Delta u_2 \end{bmatrix}^T$), representing the normal (Δv_i) and tangential (Δu_i) jumps of velocities (with respect to the discontinuity direction) evaluated on nodes $i = 1$ and $i = 2$ of the interface (see Figure 2-b). Hence, for any pair of nodes on the interface between two adjacent and coplanar triangles R and K (Figure 2-c), the tangential and normal velocity jumps can be written in terms of the Cartesian nodal velocities of elements R-K, so that four linear equations in the form $\mathbf{A}_{11}^{eq} \mathbf{w}^R + \mathbf{A}_{12}^{eq} \mathbf{w}^K + \mathbf{A}_{13}^{eq} \Delta \mathbf{u}^I = \mathbf{0}$ can be written, where $\mathbf{w}^R$ and $\mathbf{w}^K$ are the 9×1 vectors that collect velocities of elements R and K respectively and $\mathbf{A}_{1j}^{eq}$ $j = 1, 2, 3$ are matrices which depend only on the interface orientation Ω^I.

Under in-plane loads three equality constrains representing the plastic flow in the continuum (obeying an associated flow rule) are introduced for each element in the form $\dot{\boldsymbol{\varepsilon}}_{pl}^E = \dot{\lambda}^E \partial S^{\mathrm{hom}} / \partial \boldsymbol{\Sigma}$, where $\dot{\boldsymbol{\varepsilon}}_{pl}^E$ is the plastic strain rate vector of element E, $\dot{\lambda}^E \geq 0$ is the plastic multiplier, S^{hom} is the homogenised (non) linear failure surface of masonry and $\boldsymbol{\Sigma}$ is the vector of macroscopic variables $\boldsymbol{\Sigma} = (N_{11}, N_{12}, N_{22}, M_{11}, M_{12}, M_{22})$.

From the previous section, a linear approximation (with m hyper-planes) of the failure surface in the form $S^{\mathrm{hom}} \equiv \mathbf{A}^{in} \boldsymbol{\Sigma} \leq \mathbf{b}^{in}$ is considered, where $\mathbf{A}^{in}$ is a $m \times 6$ matrix of coefficients of each hyper-plane and $\mathbf{b}^{in}$ is a $m \times 1$ vector of the right hand sides of the linear approximation. Note that three linear equality constraints per element can be written ($\mathbf{A}_{11}^{eq} \mathbf{w}^E + \mathbf{A}_{12}^{eq} \dot{\boldsymbol{\lambda}}^E = \mathbf{0}$, where $\mathbf{w}^E$ is the vector of element velocities and $\dot{\boldsymbol{\lambda}}^E$ is a $m \times 1$ vector of plastic multiplier rates, one for each plane of the linearised failure surface).

Due to the linear interpolation of the velocity field, out-of-plane plastic dissipation occurs only along each interface I between two adjacent triangles R and K or on a boundary side B of an element Q (see Figure 3). Denoting with $\mathbf{w}_{zz,E} = \begin{bmatrix} w_{zz}^{i(E)} & w_{zz}^{j(E)} & w_{zz}^{k(E)} \end{bmatrix}^T$ the element E out-of-plane nodal velocities and with $\dot{\boldsymbol{\theta}}_E = \begin{bmatrix} \dot{\vartheta}_i^E & \dot{\vartheta}_j^E & \dot{\vartheta}_k^E \end{bmatrix}^T$ the side normal rotation rates, it is possible to show that $\dot{\boldsymbol{\theta}}_E$ and $\mathbf{w}_{zz,E}$ are linked by the compatibility equation (Figure 3) $\dot{\boldsymbol{\theta}}_E = \mathbf{B}_E \mathbf{w}_{zz,E}$, where $\mathbf{B}_E$ is a 3x3 matrix that depends only on the geometry of element E.

The total internal power dissipated P^{in} is constituted by the power dissipated in continuum, P_E^{in}, and the power dissipated on interfaces, P_I^{in}. P_E^{in} can be evaluated

for each triangle E of area A_E taking into account that curvature rates $\dot{\chi}_{xx}$, $\dot{\chi}_{xy}$, $\dot{\chi}_{yy}$ are zero in continuum, so that the flexural part of the model does not dissipate power in the continuum.

For an interface I of length Γ and orientation Ω^I, a rotation operator is applied to the linearized homogenised failure surface in order to obtain with a few row operations m equations (one for each hyper-plane representing the homogenised failure surface $\widetilde{S}^{\,\mathrm{hom}}$ in the $\mathbf{n}-\mathbf{t}$ interface frame of reference, Figure 2-b). Therefore, the power dissipated P_I^{in} along an interface I of length Γ and with orientation Ω^I can be estimated as $P_I^{in} = \int_\Gamma \sum_{q=1}^m C_I^q \dot{\lambda}_I^{(q)}(\xi) d\xi$, where $\dot{\lambda}_I^{(q)}(\xi)$ represents the qth plastic multiplier rate of a point ξ of the interface I and C_I^q is the right hand side of the qth linearization plane of the homogenized failure surface of the interface.

In the model, the possible presence of ring and RC/steel beams is also considered through the utilization of suitable two-node beam elements (see Figure 2-c). A linear interpolation of the velocity field inside the elements is adopted. Thus, plastic dissipation inside each beam is due only to normal action (compression or tension), whereas flexural dissipation occurs only at the interfaces between adjoining elements. No dissipation occurs for torsion. We suppose for the sake of simplicity that ultimate axial load $N_u^{+/-}$ (+: tension, -: compression) and bending moments along perpendicular principal directions of the beam section ($M_{u\xi}$ and $M_{u\eta}$) are uncoupled. Therefore internal plastic dissipation on beam elements is given by a contribution of the element (P_B^{in}) due to N_u and a contribution of the plastic hinge between two elements (P_N^{in}) due to M_u.

For what concerns external power dissipation, no differences occur with respect to classic FE limit analysis codes. External power dissipated can be written as $P^{ex} = \left(\mathbf{P}_0^T + \lambda \mathbf{P}_1^T\right)\mathbf{w}$, where $\mathbf{P}_0$ is the vector of (equivalent lumped) permanent loads, λ is the load multiplier for the structure examined, $\mathbf{P}_1^T$ is the vector of (lumped) variable loads and $\mathbf{w}$ is the vector of assembled nodal velocities. As the amplitude of the failure mechanism is arbitrary, a further normalization condition $\mathbf{P}_1^T \mathbf{w} = 1$ is usually introduced. Hence, the external power becomes linear in $\mathbf{w}$ and λ, i.e. $P^{ex} = \mathbf{P}_0^T \mathbf{w} + \lambda$.

After some assemblage operations (not reported for the sake of conciseness), the following linear programming problem is obtained (analogous to that reported elsewhere [13]), where the objective function consists of the minimization of the total internal power dissipated:

$$\min\left\{\sum_{I=1}^{n^I} P_I^{in} + \sum_{E=1}^{n^E} P_E^{in} - \mathbf{P}_0^T \mathbf{w}\right\} \text{ such that } \begin{cases} \mathbf{A}^{eq}\mathbf{U} = \mathbf{b}^{eq} \\ \dot{\boldsymbol{\lambda}}^{I,ass} \geq \mathbf{0} \quad \dot{\boldsymbol{\lambda}}^{E,ass} \geq \mathbf{0} \\ \dot{\boldsymbol{\theta}}^{ass} = \dot{\boldsymbol{\theta}}^+ - \dot{\boldsymbol{\theta}}^- \\ \dot{\boldsymbol{\theta}}^+ \geq 0 \quad \dot{\boldsymbol{\theta}}^- \geq 0 \end{cases} \quad (4)$$

where:

- $\mathbf{U}$ is the vector of global unknowns and collects the vector of assembled nodal velocities ($\mathbf{w}$), the vector of assembled element plastic multiplier rates ($\dot{\boldsymbol{\lambda}}^{E,ass}$), the vector of assembled jump of velocities on interfaces ($\Delta\mathbf{u}^{I,ass}$), the vector of assembled interface plastic multiplier rates ($\dot{\boldsymbol{\lambda}}^{I,ass}$) and the vector of interface and boundary out-of-plane rotation angles $\dot{\boldsymbol{\theta}}^{ass}$;

- $\mathbf{A}^{eq}$ is the overall constraints matrix and collects normalization conditions, velocity boundary conditions, relations between velocity jumps on interfaces and elements velocities, constraints for plastic flow in velocity discontinuities and constraints for plastic flow in continuum.

- n^E and n^I are the total number of elements and interfaces, respectively.

4 Structural level. Failure loads prediction of a 3D masonry structure.

The example treated in this Section consists in the prediction of the horizontal failure load of a real three storey masonry building located in Italy, see Figure 4. The building is a school erected in the north-east of Italy at the end of 19th century, in an isolated position and consisting of two structurally independent rectangular main bodies, as shown in the plan view reported in Figure 5.

The main building, called here for the sake of simplicity Body A, presents a rectangular shape with dimensions $L_1 \times L_2 = 49.0 \times 12.2$ m^2 and 3 storeys, whereas the secondary Body B has a rectangular shape $L_1 \times L_2 = 8 \times 13$ m^2 and 3 storeys. All the walls are made with clay bricks, assumed of dimensions $250 \times 120 \times 55$ mm^3 (length $\times$ width $\times$ height) in absence of precise information. The first storey height is 4.85 m whereas the second and third storeys height is 4.65 m.

A rehabilitation intervention was carried out during the 1980's. In that occasion, several bearing walls at the ground floor level were removed and replaced by steel beams at the first floor level, with the aim of sustaining gravity loads (until recent years, the school was not in seismic area according to the Italian code). Furthermore, a 20 mm separation joint was introduced between Body A and B. Therefore, it is reasonable to consider two substructures which behave separately under horizontal actions. Here, only Body A is taken into consideration for the sake of conciseness.

Body A is geometrically regular with equally distributed mass, except for the large openings at the centre of the first floor of the three walls parallel to x direction, which are part of a corridor giving access to the building. A main corridor of access to classrooms is located between walls x-1 and x-2, Figure 5. Walls thickness is reported in Table 1.

A FE model consisting of 1576 triangular elements is used for performing the homogenised limit analysis proposed (Figure 4-a) under a static equivalent seismic load directed along x-direction. Rigid-plastic beam elements have been used to simulate steel beams in correspondence of first floors under walls y-3. The results obtained with the homogenised FE limit analysis model (i.e. failure shear at the base and failure mechanism) are compared with a standard FE elastic-perfectly plastic

analysis conducted by means of a commercial FE software (Strand 7). The analysis is performed using a mesh of 3152 four-node shell elements supposing masonry isotropic with a Mohr-Coulomb failure criterion.

For masonry, a cohesion c equal to 0.12 N/mm^2 and friction angle $\Phi = \tan^{-1}(0.4)$ are adopted for the simulations, in agreement with the Italian code [2,3]. In order to compare the homogenised limit analysis procedure proposed with the standard FE model, a linearized Lourenço-Rots [5] failure criterion for joints is adopted for the homogenisation approach, whereas for units a cut-off failure criterion in compression is assumed, see Table 2.

In both models, the seismic load is applied in correspondence of floor i by means of a horizontal distributed load of intensity $k_i\hat{\lambda}$ (k_i non-dimensional constant), where $\hat{\lambda}$ is the collapse load and k_i is taken, in agreement with the Italian code [2,14], equal to $z_iW_i/\left(\sum z_iW_i\right)$, where W_i is the i th floor vertical load, z_i is the i th floor distance to the ground and the summation is extended to the total number of floors.

Floors, constituted by small vaults made of clay bricks and supported by a framework of steel girders, are disposed parallel to y-direction in correspondence to the first and second floors and distribute vertical loads uniformly on x-directed walls. As a first attempt, floors stiffness is not taken into account in the numerical model and vertical loads, which are independent from the load multiplier, are applied directly on masonry walls in correspondence to the floors. In correspondence of the third floor, a timber truss structure supports an inclined roof covering. For the sake of simplicity, self weight of masonry is supposed concentrated in correspondence to the floors and added to the remaining dead loads, which are defined according to the Italian code [14, 15, 16]).

The kinematic FE homogenised limit analysis gives a total shear at the base of the building of 3520 kN, in good agreement with the results obtained with the standard FE procedure. In this case, in fact, the capacity curve of the building, Figure 6-a, reaches its maximum at approximately 3800kN. Finally, the deformed shape at collapse of both models, compare Figure 6-b and Figure 7, demonstrates that a combined in- and out-of-plane failure takes place and that failure is mainly concentrated along walls x-2 and x-3.

A sensitivity analysis is finally conducted, assuming for joints a classic Mohr-Coulomb failure criterion with tension cut-off f_t equal to $\min\left\{0.05\,\text{N/mm}^2 \quad c/\tan\Phi\right\}$, compressive cut-off $f_t = 5\text{N/mm}^2$ and varying cohesion c and friction angle Φ in the range 0.01-0.5N/mm^2 and 5-35°. For bricks a limited compressive strength equal to 30 N/mm^2 is also assumed.

In Figure 8, the failure load of the structure is reported varying mortar cohesion and friction angle. From an overall analysis of sensitivity results, two different failure mechanisms can be distinguished, labelled as failure mechanism A and B. The intervals in which they take place are indicated schematically in Figure 8. In particular, mechanisms A, reported in Figure 7, corresponds to an in-plane failure of walls x-2 and x-3 combined with an out-of-plane failure of walls y-1. On the other hand, Mechanism B, reported in Figure 9, combines a shear failure of wall x-2 concentrated on the second storey and overturning of walls y-1. Finally, from an

overall analysis of the results, it is worth noting that only a homogenized rigid plastic approach (as that proposed in the present paper) allows to perform sensitivity ~~analysis~~ analyses (1) very quickly (less than 120 seconds are needed for each simulation on a standard PC with 2Gb Ram) and (2) taking into consideration important distinctive aspects of masonry behaviour at failure, as for instance the anisotropy along material axes. Analyses performed with standard non-linear FE codes are always time consuming and commercial codes have rarely at disposal routines devoted to the masonry study at failure.

5   Conclusions

A 3D FE upper bound limit analysis code based on homogenization has been presented. The software is based on a plate and shell discretization of masonry piers and spandrels. The possible presence of 1D beams is modelled by means of two-node rigid beam elements. Homogenized masonry failure surfaces are utilized in the software. They are obtained subdivided the elementary cell along its thickness into several layers. For each layer, fully equilibrated stress fields are assumed, adopting polynomial expressions for the stress tensor components in a finite number of sub-domains.

The structural model allows plastic dissipation for in-plane actions on triangular elements and on interfaces, whereas out-of-plane yield lines are concentrated only at the interfaces between contiguous elements.

To validate the software, a relevant 3D structural example consisting on a masonry school subjected to horizontal actions has been treated. Full sensitivity analyses and a comparison with results obtained with a commercial elasto-plastic software have been presented, indicating the good performance of the model.

References

1   GIUFFRÈ A. (Editor). Safety and conservation of historical centers: the Ortigia case. *Laterza Press, Roma - Bari*, *Italy*, 1993 [in Italian].

2   O.P.C.M. 3274, 20/03/2003. First elements concerning general criteria for the seismic classification of the national territory and technical norms for structures in seismic zone [in Italian, Primi elementi in materia di criteri generali per la classificazione sismica del territorio nazionale e di normative tecniche per le costruzioni in zona sismica], 2003.

3   O.P.C.M. 3431/05 09/05/2005. Further modifications and integrations on OPCM 3274/03" [in Italian, Ulteriori modifiche ed integrazioni all'OPCM 3274/03], 2003.

4   LOURENÇO P.B. Computations of historical masonry constructions. *Progress in Structural Engineering and Materials*, 2002, **4**, No.3, 301-319.

5   LOURENÇO P.B., ROTS J. A multi-surface interface model for the analysis of masonry structures. *Journal of Engineering Mechanics ASCE*, 1997, **123**, No. 7, 660-668.

6   LOURENÇO P.B., DE BORST R., ROTS J. A plane stress softening plasticity model for orthotropic materials. *International Journal for Numerical Methods in Engineering*, 1997, **40**, 4033-4057.

7   SUQUET P. Analyse limite et homogeneisation. *Comptes Rendus de l'Academie des Sciences - Series IIB – Mechanics*, 1983, **296**, 1355-1358.

8   MILANI G., LOURENÇO P.B., TRALLI A. Homogenised limit analysis of masonry walls. Part II: structural examples. *Computers & Structures*, 2006, **84**, 181-195.

9   MILANI G., LOURENÇO P.B., TRALLI A. Homogenised limit analysis of masonry walls. Part I: failure surfaces. *Computers & Structures*, 2006, **84**, 166-180.

10 MILANI G., LOURENÇO P.B., TRALLI A. Homogenisation approach for the limit analysis of out-of-plane loaded masonry walls. *Journal of Structural Engineering ASCE*, 2006, **132**, No. 10, 1650-1663.

11 SLOAN S.W., KLEEMAN P.W. Upper bound limit analysis using discontinuous velocity fields. *Computer Methods in Applied Mechanics and Engineering*, 1995, **127**, No. 1-4, 293-314.

12 MUNRO J., DA FONSECA A.M.A. Yield-line method by finite elements and linear programming. *Journal of Structural Engineering ASCE*, 1978, **56B**, 37-44.

13 KRABBENHOFT K., LYAMIN A.W., HJIAJ M., SLOAN S.W. A new discontinuous upper bound limit analysis formulation. *International Journal for Numerical Methods in Engineering*, 2005, **63**, 1069-1088.

14 D.M. 16/01/1996 (G.U. 5-2-1996, N. 29). Technical norms relative to "general criteria for the safety assessment of structures and loads" [in Italian, Norme tecniche relative ai "Criteri generali per la verifica di sicurezza delle costruzioni, e dei carichi e sovraccarichi"].

15 BRENCICH A., GAMBAROTTA L., LAGOMARSINO S. Catania project: research on the seismic response of two masonry buildings. Chapter 6: Analysis of a masonry building in via Martoglio. *CNR Gruppo Nazionale per la Difesa dei Terremoti (editor)*, 2000, 107-151 [in Italian].

16 MAGENES G., BRAGGIO C. Catania project: research on the seismic response of two masonry buildings. Chapter 7: analysis of a masonry building in via Martoglio. *CNR Gruppo Nazionale per la Difesa dei Terremoti (editor)*, 2000, 153-190 [in Italian]

Tables

storey	x-1	x-2	x-3	y-1	y-2	y-3
1	60	45	60	60	45	-
2	50	45	50	50	45	45
3	45	30	45	45	30	30

Table 1: Entire masonry building subjected to horizontal actions. Walls thickness (cm)

Joint				Brick
c [N/mm^2]	f_t [N/mm^2]	f_c [N/mm^2]	Φ_1	f_c [N/mm^2]
0.12	0.12	5	35°	30
Cohesion	Tensile strength	Compressive strength	Friction angle	Compressive strength

Table 2: Entire masonry building subjected to horizontal actions. Mechanical characteristics assumed for joints and bricks
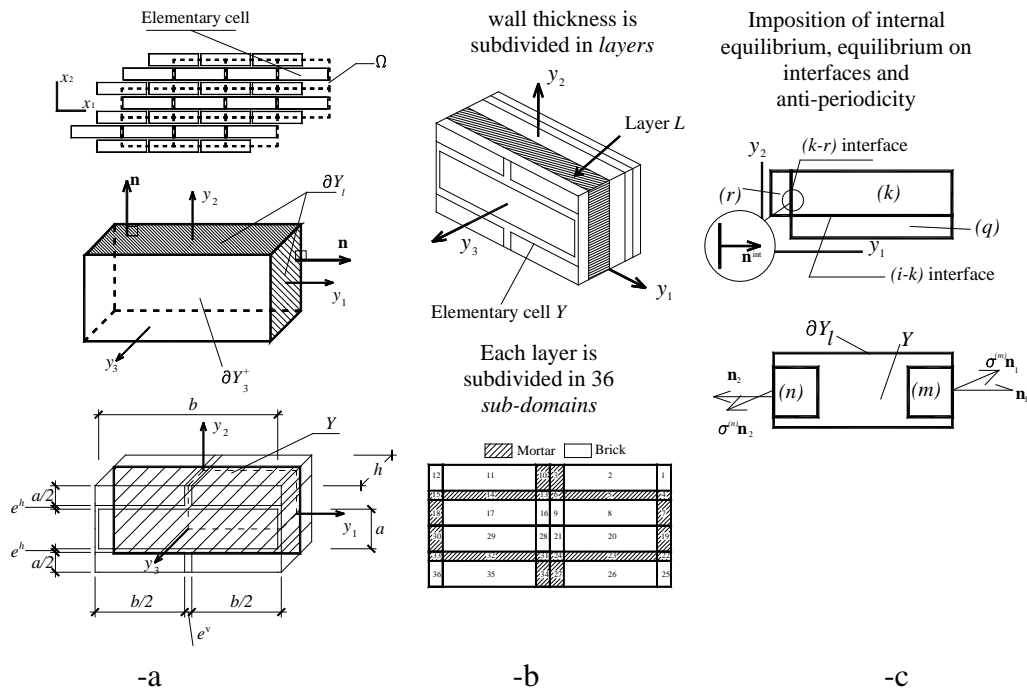
Figures

Figure 1: Proposed micro-mechanical model. -a: elementary cell. -b: subdivision in layers along thickness and subdivision of each layer in sub-domains. -c: imposition of internal equilibrium, equilibrium on interfaces and anti-periodicity
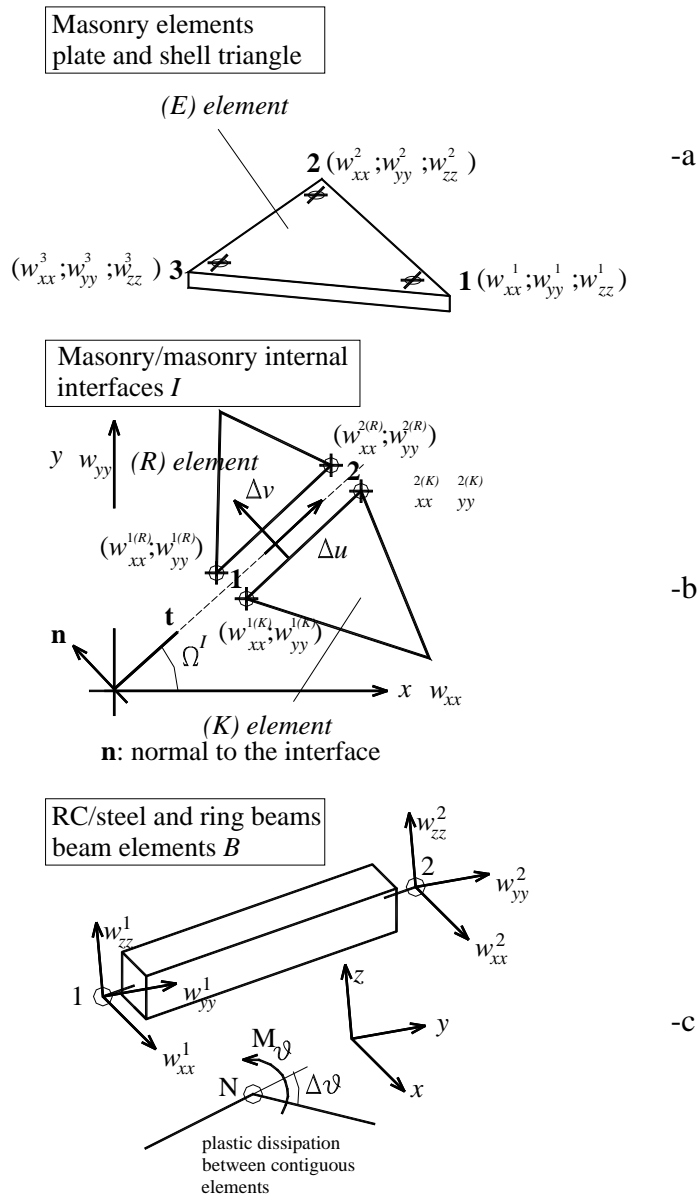
Masonry elements
plate and shell triangle

(E) element

$2\,(w_{xx}^{2};w_{yy}^{2};w_{zz}^{2})$

-a

$(w_{xx}^{3};w_{yy}^{3};w_{zz}^{3})\,\mathbf{3}$

$\mathbf{1}\,(w_{xx}^{1};w_{yy}^{1};w_{zz}^{1})$

Masonry/masonry internal
interfaces *I*

$(w_{xx}^{2(R)};w_{yy}^{2(R)})$

$y\;\;w_{yy}$ *(R) element*

Δv $\mathbf{2}$

$\begin{matrix}2(K) & 2(K)\\ xx & yy\end{matrix}$

$(w_{xx}^{1(R)};w_{yy}^{1(R)})$

Δu

$\mathbf{1}$

-b

$\mathbf{n}$

$\mathbf{t}$

Ω^{I} $(w_{xx}^{1(K)};w_{yy}^{1(K)})$

$x\;\;w_{xx}$

(K) element
$\mathbf{n}$: normal to the interface

RC/steel and ring beams
beam elements *B*

w_{zz}^{2}

2

w_{yy}^{2}

w_{zz}^{1}

w_{xx}^{2}

1 w_{yy}^{1}

z

w_{xx}^{1}

y

-c

M_{ϑ}

N $\Delta\vartheta$

x

plastic dissipation
between contiguous
elements

Figure 2: -a: Triangular plate and shell element used for the upper bound FE limit analysis. -b: discontinuity of the in-plane velocity field. -c: finite elements used to model ring beams and steel/RC beams.
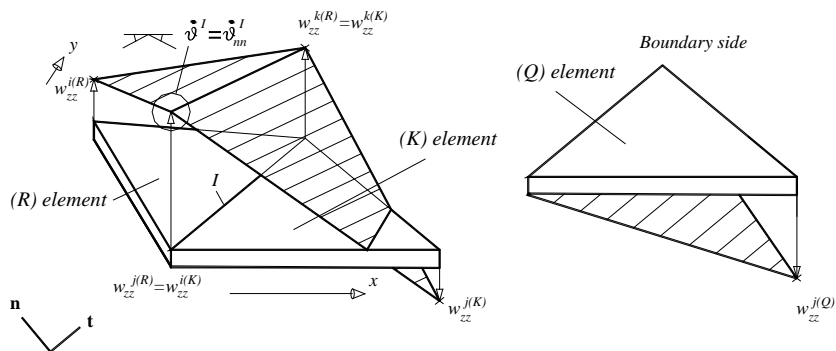
Figure 3: Rotation rate along an interface between adjacent triangles or in correspondence of a boundary side

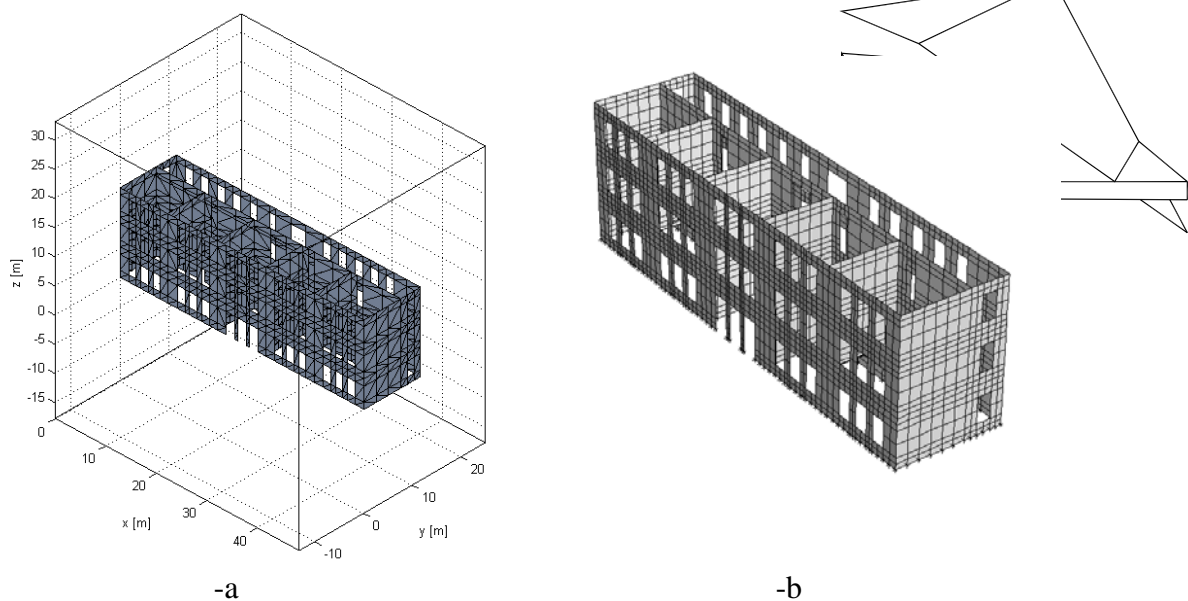-a   -b

Figure 4: Entire masonry building subjected to horizontal actions. -a: Mesh used for the limit analysis (1576 triangular elements) and (-b) mesh used in Strand 7 for an elastic-plastic analysis with Mohr-Coulomb failure criterion (3152 plate elements)
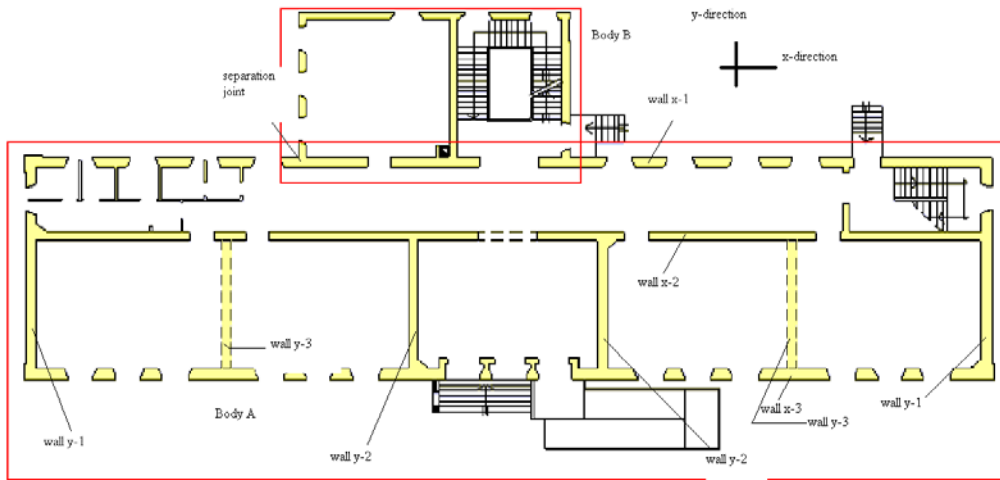
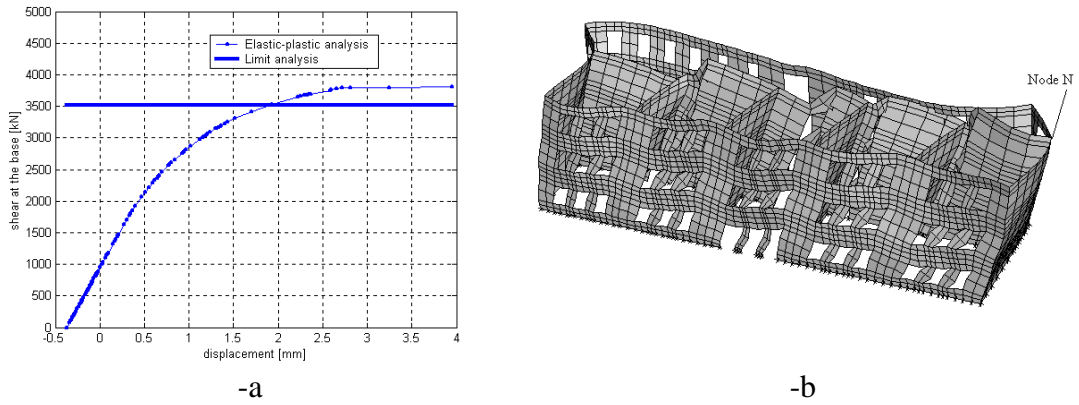Figure 5: First floor plan view, masonry building subjected to horizontal action

-a   -b

Figure 6: Masonry building subjected to horizontal actions. Standard FE elastic plastic approach. –a: shear at the base - node N displacement curve. -b: deformed shape at collapse
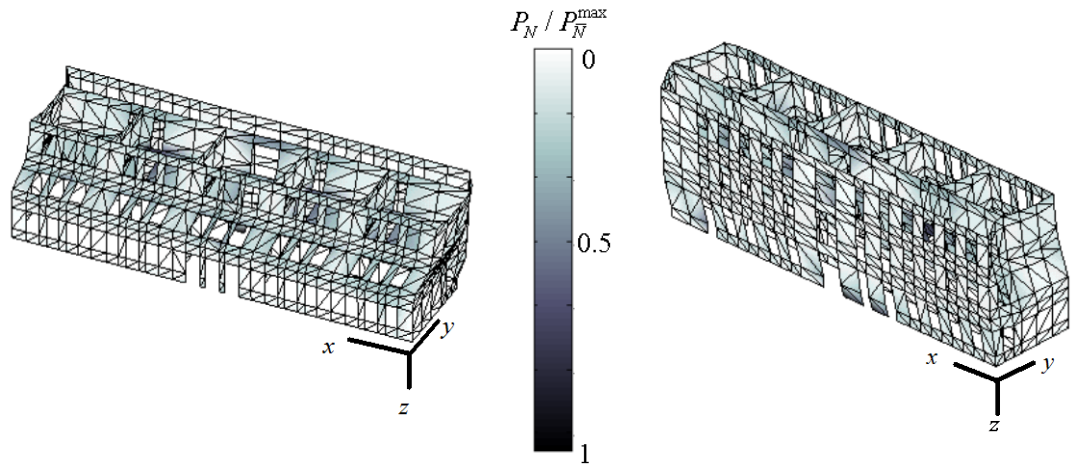

Figure 7: Masonry building subjected to horizontal actions. Two views of failure mechanism A and concentration of plastic dissipation for the entire building, homogenisation FE limit analysis approach. P_N is the in-plane plastic dissipation evaluated at node N and $\overline{N}$ is the node of maximum dissipation
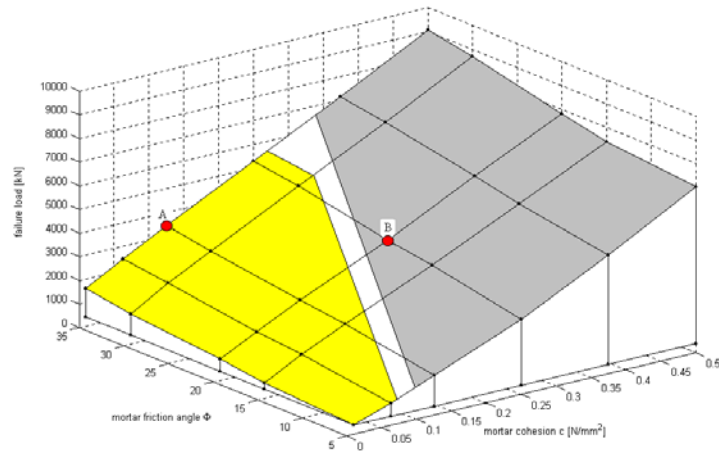
17

Figure 8: Masonry building subjected to horizontal actions. Sensitivity analysis varying mortar cohesion and mortar friction angle and failure mechanisms patch

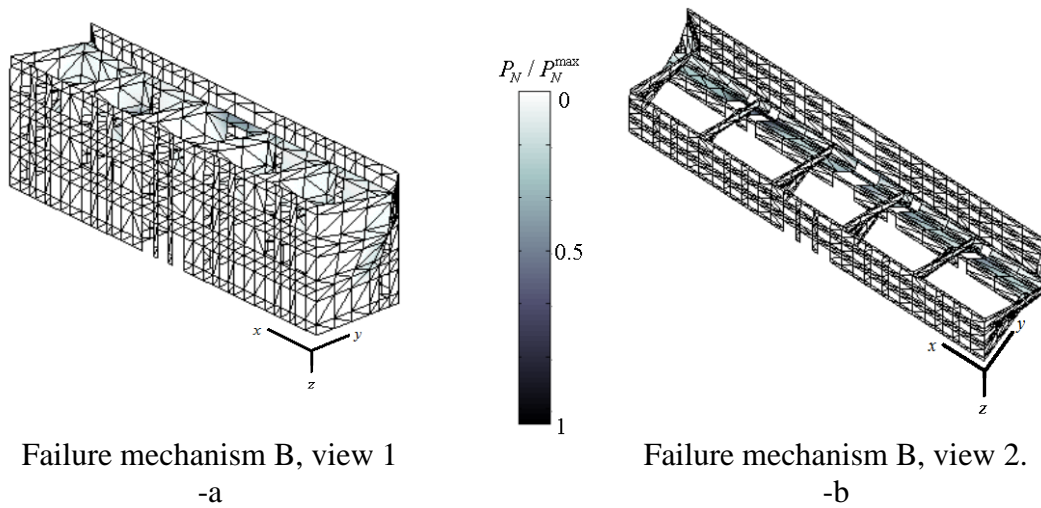| Failure mechanism B, view 1 | Failure mechanism B, view 2. |
| -a | -b |

Figure 9: Masonry building subjected to horizontal actions. Failure mechanisms B. P_N is the in-plane plastic dissipation evaluated at node N and $\overline{N}$ is the node of maximum dissipation.